

MALARIA

Functional human IgA targets a conserved site on malaria sporozoites

Joshua Tan^{1*†}, Hyeseon Cho^{2†}, Tossapol Pholcharee^{3†}, Lais S. Pereira⁴, Safiatou Doumbo⁵, Didier Doumtabe⁵, Barbara J. Flynn⁴, Arne Schön⁶, Sachie Kanatani⁷, Samantha O. Aylor⁸, David Oyen³, Rachel Vistein⁴, Lawrence Wang⁴, Marlon Dillon⁴, Jeff Skinner², Mary Peterson², Shanping Li², Azza H. Idris^{4,9}, Alvaro Molina-Cruz¹⁰, Ming Zhao¹¹, Lisa Renee Olano¹¹, Patricia J. Lee⁸, Alison Roth⁸, Photini Sinnis⁷, Carolina Barillas-Mury¹⁰, Kassoum Kayentao⁵, Aissata Ongoiba⁵, Joseph R. Francica⁴, Boubacar Traore⁵, Ian A. Wilson^{3,12‡}, Robert A. Seder^{4‡}, Peter D. Crompton^{2*‡}

Immunoglobulin (Ig)A antibodies play a critical role in protection against mucosal pathogens. However, the role of serum IgA in immunity to nonmucosal pathogens, such as *Plasmodium falciparum*, is poorly characterized, despite being the second most abundant isotype in blood after IgG. Here, we investigated the circulating IgA response in humans to *P. falciparum* sporozoites that are injected into the skin by mosquitoes and migrate to the liver via the bloodstream to initiate malaria infection. We found that circulating IgA was induced in three independent sporozoite-exposed cohorts: individuals living in an endemic region in Mali, malaria-naïve individuals immunized intravenously with three large doses of irradiated sporozoites, and malaria-naïve individuals exposed to a single controlled mosquito bite infection. Mechanistically, we found evidence in an animal model that IgA responses were induced by sporozoites at dermal inoculation sites. From malaria-resistant individuals, we isolated several IgA monoclonal antibodies that reduced liver parasite burden in mice. One antibody, MAD2-6, bound to a conserved epitope in the amino terminus of the *P. falciparum* circumsporozoite protein, the dominant protein on the sporozoite surface. Crystal structures of this antibody revealed a unique mode of binding whereby two Fabs simultaneously bound either side of the target peptide. This study reveals a role for circulating IgA in malaria and identifies the amino terminus of the circumsporozoite protein as a target of functional antibodies.

INTRODUCTION

Malaria remains an enormous public health threat among the world's most vulnerable populations. In 2019 alone, there were an estimated 229 million cases of malaria resulting in 409,000 deaths (1). Most deaths occur among children and pregnant women in sub-Saharan Africa and are caused by the *Plasmodium falciparum* parasite, the deadliest of the five *Plasmodium* species that infect humans (1). Infection begins when *Anopheles* mosquitoes inject a small number of sporozoites into the skin. Sporozoites rapidly migrate to the liver

via the bloodstream and infect hepatocytes where they differentiate into merozoites and replicate without causing symptoms. After approximately 7 days, merozoites rupture out of hepatocytes into the bloodstream and infect and replicate within erythrocytes in a 48-hour cycle that rapidly increases the number of blood-stage parasites and causes an acute, potentially life-threatening illness. In endemic areas, clinical immunity that protects from blood-stage disease can be acquired after years of repeated infections, although sterilizing immunity that prevents the progression to blood-stage infection appears to be rare (2, 3). The development of resistance to antimalarial medicines and insecticides is a perpetual challenge that jeopardizes efforts to control and eliminate malaria. The most clinically advanced malaria vaccine candidate, RTS,S, conferred up to 56% protection from clinical malaria after the first year and up to 36% protection at 3 to 4 years in those who received a booster (4–6), underscoring the need to develop additional tools and approaches by examining different facets of immunity against the malaria parasite.

Antibodies can play a critical role in mediating protection against all stages of malaria (7). The vast majority of studies on the antibody response to *P. falciparum* have focused on the immunoglobulin (Ig) G or IgM isotypes (7–11) based on the fact that most neutralization of *P. falciparum* occurs in the blood. In contrast, IgA antibodies are thought to play a much larger role in protection against mucosal pathogens (12). However, IgA is the second most abundant antibody isotype in blood after IgG, and the role of circulating IgA is poorly characterized (13). To investigate whether circulating IgA aids in defense against nonmucosal pathogens, we studied the IgA response to *P. falciparum* whose life cycle in humans is limited to nonmucosal organs. We examined the IgA response to *P. falciparum*

¹Antibody Biology Unit, Laboratory of Immunogenetics, National Institute of Allergy and Infectious Diseases (NIAID), National Institutes of Health (NIH), Rockville, MD 20852, USA. ²Malaria Infection Biology and Immunity Section, Laboratory of Immunogenetics, National Institute of Allergy and Infectious Diseases, National Institutes of Health, Rockville, MD 20852, USA. ³Department of Integrative Structural and Computational Biology, Scripps Research Institute, La Jolla, CA 92037, USA. ⁴Vaccine Research Center, National Institute of Allergy and Infectious Diseases, National Institutes of Health, Bethesda, MD 20892, USA. ⁵Mali International Center of Excellence in Research, University of Sciences, Technique and Technology of Bamako, BP 1805, Point G, Bamako, Mali. ⁶Department of Biology, Johns Hopkins University, Baltimore, MD 21218, USA. ⁷Department of Molecular Microbiology & Immunology, Johns Hopkins Bloomberg School of Public Health, 615 N. Wolfe Street, Baltimore, MD 21205, USA. ⁸Department of Drug Discovery, Experimental Therapeutics Branch, Walter Reed Army Institute of Research, Silver Spring, MD 20910, USA. ⁹Biological Engineering Department, Massachusetts Institute of Technology, Cambridge, MA 02139, USA. ¹⁰Laboratory of Malaria and Vector Research, National Institute of Allergy and Infectious Diseases, National Institutes of Health, Rockville, MD 20852, USA. ¹¹Protein Chemistry Section, Research Technologies Branch, National Institute of Allergy and Infectious Diseases, National Institutes of Health, Rockville, MD 20852, USA. ¹²The Skaggs Institute for Chemical Biology, The Scripps Research Institute, La Jolla, CA 92037, USA.

*Corresponding author. Email: tanj4@nih.gov (J.T.); pcrompton@niaid.nih.gov (P.D.C.)

†These authors contributed equally to this work.

‡These authors jointly supervised this work.

sporozoites in individuals living in a malaria-endemic region of Mali, as well as malaria-naïve individuals who were immunized intravenously with radiation-attenuated sporozoites or exposed to infectious mosquito bites in a controlled setting. We isolated *P. falciparum* circumsporozoite protein (PfCSP)-specific IgA monoclonal antibodies (mAbs) from two Malian individuals and investigated the fine specificity and function of these antibodies. We found that exposure to sporozoites through different routes triggered a specific IgA response. We identified an IgA mAb, MAD2-6, that bound to a conserved epitope on the N terminus of PfCSP, inhibited sporozoite invasion in vitro, and reduced liver parasite burden in vivo. These findings reveal a role for IgA in the immune response to *P. falciparum* and identify the N terminus of PfCSP as a target of functional antibodies.

RESULTS

Infection and vaccination with *P. falciparum* sporozoites induce IgA antibodies that target PfCSP

We first examined the IgA response to natural *P. falciparum* infection in a cohort study conducted in a region of Mali where the annual malaria season is clearly defined (fig. S1A). To detect long-lasting antibodies, we screened plasma collected from 758 individuals after the 5-month dry season (a period of negligible malaria transmission) for binding to *P. falciparum* NF54 sporozoites and a mixture of infected erythrocytes representing four parasite strains. In contrast to muted IgA responses to infected erythrocytes, many plasma samples showed IgA binding to sporozoites (Fig. 1A). We observed a significant correlation ($r = 0.5426$, $P < 0.0001$) between IgA binding to *P. falciparum* sporozoites and PfCSP (fig. S1B), consistent with the immunodominance of PfCSP on the sporozoite surface. We found a weaker correlation between IgA and IgG binding to sporozoites ($r = 0.2627$, $P < 0.0001$) (fig. S1B). Segmented regression analysis of the relationship between sporozoite-specific IgA and age revealed a breakpoint at 12.5 years (fig. S1B), and correlation analysis before and after this breakpoint showed that IgA binding to sporozoites increased slightly up to about 12 years of age ($r = 0.2133$, $P < 0.0001$) and then plateaued ($r = -0.024$; $P = 0.670$) (fig. S1B). To investigate whether acute *P. falciparum* infection boosts IgA responses to sporozoites in previously infected individuals, we analyzed 10 Malian children aged 7 to 8 years with confirmed prior infections for their sporozoite-specific IgA, IgG, and IgM response before, during, and after a febrile malaria episode (fig. S1C). Although the effect was more pronounced for IgG and IgM, we found that sporozoite-specific IgA increased in 6 of 10 individuals in response to infection. To estimate the relative frequency of PfCSP-specific IgA⁺ and IgG⁺ memory B cells in malaria-experienced individuals, we isolated and polyclonally activated the respective B cell subsets from 50 Malian individuals and screened the supernatants for binding to PfCSP and Pf merozoite surface protein-1 (MSP-1) as a blood-stage antigen comparator. Of the 1.5×10^6 IgA⁺ (598 wells) and 7.0×10^6 IgG⁺ (2720 wells) memory B cells screened, we identified 37 positive PfCSP-specific IgA wells (6.2% of wells) and 96 positive PfCSP-specific IgG wells (3.5% of wells) (fig. S1D). In contrast, for PfMSP-1, we identified 29 positive IgA wells (4.8%) and 826 positive IgG wells (30.4%). Collectively, these data suggest that natural *P. falciparum* infection can trigger the generation of anti-sporozoite IgA antibodies and PfCSP-specific memory B cells.

We also measured sporozoite-specific IgG, IgM, and IgA in plasma samples of 43 malaria-naïve U.S. adults (fig. S2A). Several individuals

had high amounts of sporozoite-specific IgG and, overall, these individuals had amounts of IgA and IgM binding to sporozoites that were comparable to the Malian responses, presumably due to pre-existing B cells primed by non-*Plasmodium* antigens whose antibodies cross-react with sporozoite surface antigens (14). To determine whether exposure to sporozoites triggers a specific IgA response in malaria-naïve individuals, we screened longitudinal plasma samples from a clinical trial (VRC 314) in which malaria-naïve U.S. individuals were immunized intravenously with three doses of irradiated, aseptic, cryopreserved *P. falciparum* NF54 sporozoites (Sanaria PfSPZ Vaccine) before controlled human malaria infection (CHMI) with *P. falciparum* 3D7-infected mosquitoes. The PfSPZ Vaccine induced an IgA response against sporozoites and PfCSP (Fig. 1B and fig. S2B), consistent with a study reporting PfCSP-specific IgA in serum after immunization with sporozoites under chemoprophylaxis (14). The sporozoite-specific IgA targeted the immunodominant NANP repeat region and remained stably elevated in four of five individuals over a year that included a 4-month period without sporozoite exposure (fig. S2B), suggesting that long-lived IgA⁺ plasma cells were generated in these individuals. PfCSP-specific IgA⁺ memory B cells were also detected 3 months after the final immunization (Fig. 1C and fig. S2, C and D).

We also examined malaria-naïve individuals who were exposed to the bites of five *P. falciparum* 3D7-infected mosquitoes through CHMI without prior immunization. Exposure to a single infection dose induced sporozoite-specific plasma IgA, with 6 of 14 individuals evaluated reaching a greater than twofold increase in antibody binding (Fig. 1D), confirming that the natural route of sporozoite transmission induces IgA antibodies. As expected, we also observed an ant sporozoite IgG response in the PfSPZ Vaccine-immunized and infected mosquito-exposed individuals. In the immunized individuals, the IgG response peaked later and plateaued at a higher baseline than IgA (fig. S2E), whereas the group exposed only to *P. falciparum*-infected mosquitoes displayed a similar IgG response to IgA in terms of the specific individuals that responded, as well as the kinetics and magnitude of the response (fig. S2F).

To determine the initial site of IgA class switching after sporozoite exposure, we used a mouse model that allowed us to control the site of sporozoite delivery. We injected the left ear of BALB/c mice intradermally with transgenic *P. berghei* sporozoites that express PfCSP in place of *P. berghei* CSP (Pb-PfCSP). Six days later, NANP-specific IgA⁺ plasmablasts were detected in the draining ipsilateral auricular lymph node (LN) and spleen, but not in the contralateral auricular LN, portal/cealic LNs, mesenteric LNs, or Peyer's patches (Fig. 1E and fig. S3), the latter two being intestinal sites traditionally associated with IgA⁺ B cell class switching. Control mice injected with salivary gland extract from uninfected mosquitoes did not generate NANP-specific responses (Fig. 1E). These findings are consistent with reports of sporozoite entry into LNs draining skin inoculation sites (15) and suggest that sporozoites induce IgA responses at these locations.

Isolation and characterization of IgA mAbs targeting PfCSP

To study the human IgA response at higher resolution, we established a protocol to isolate IgA anti-CSP mAbs from individuals in the Mali cohort. We downselected donors on the basis of two criteria. First, we identified donors who were *P. falciparum* blood-stage negative by polymerase chain reaction (PCR) every time that they were tested as a possible indication of resistance to sporozoite infection.

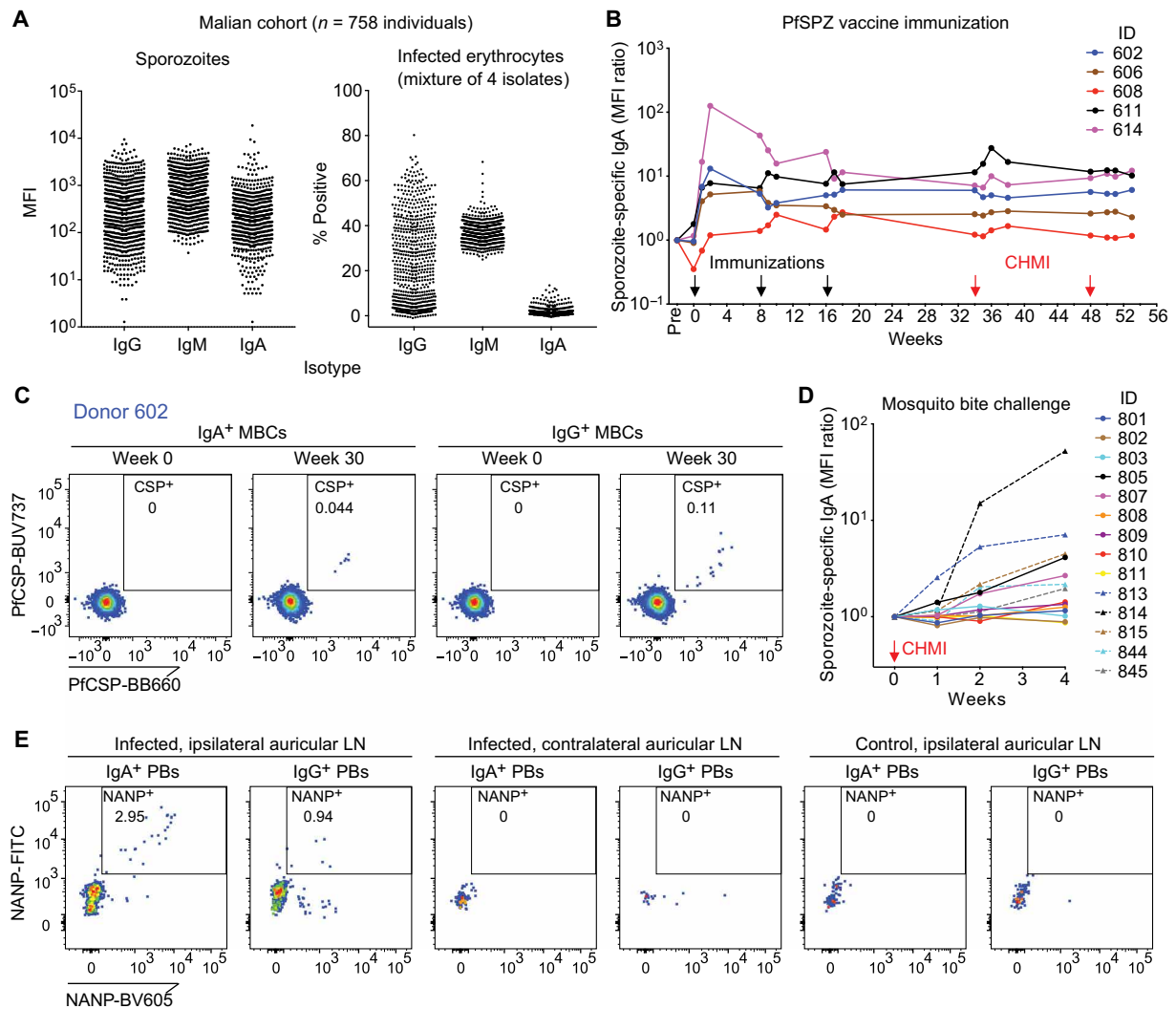


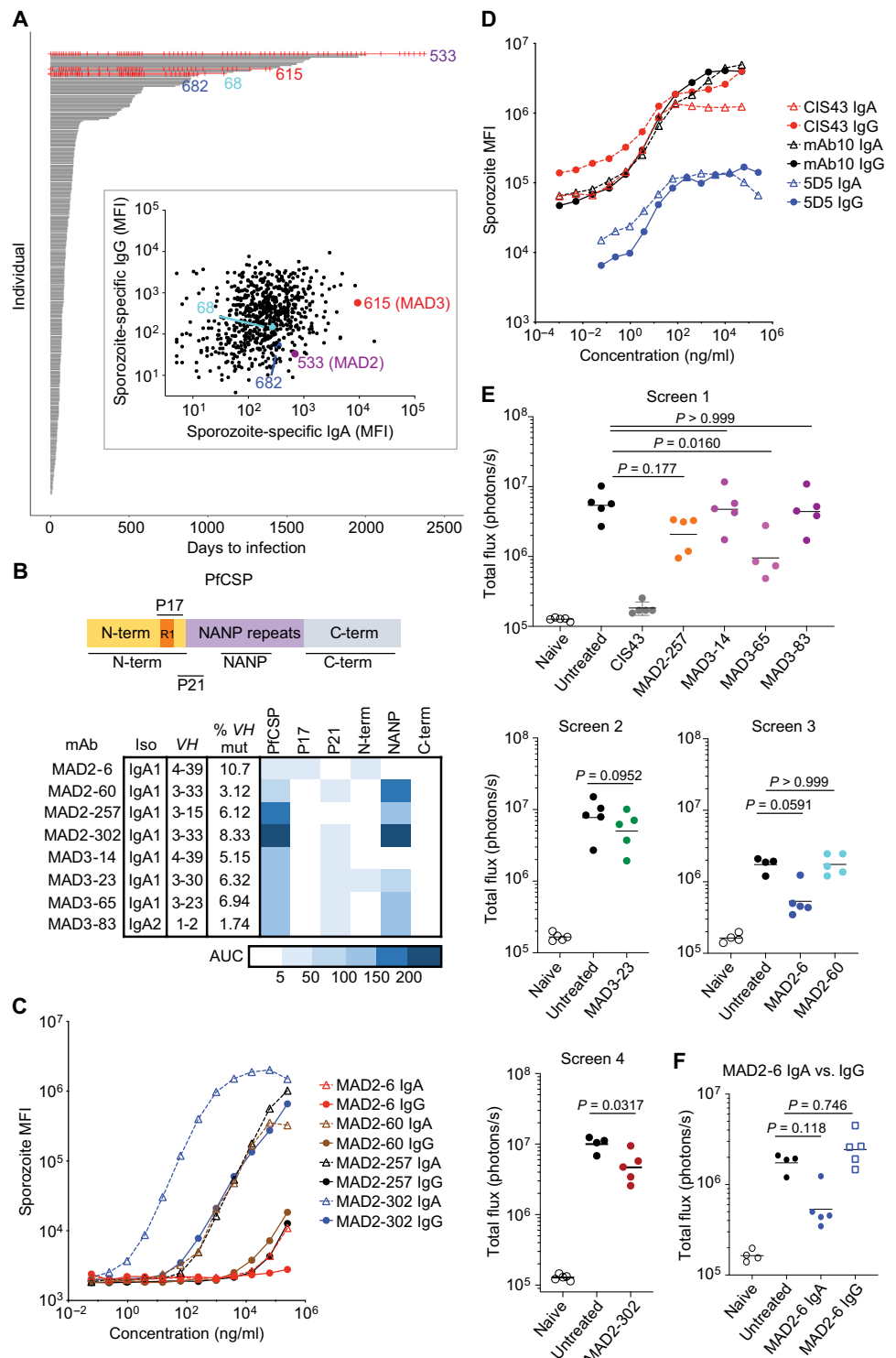
Fig. 1. Infection and vaccination with *P. falciparum* sporozoites induces a long-lasting IgA response. (A) Binding of plasma IgG, IgM, and IgA to *P. falciparum* sporozoites and infected erythrocytes among 758 Malian individuals ($N=2$ experiments for sporozoites; $N=1$ for infected erythrocytes). MFI, median fluorescence intensity. (B) Sporozoite-specific plasma IgA responses in U.S. volunteers after immunization with $3 \times 900,000$ cryopreserved, irradiated *P. falciparum* sporozoites (Sanaria PfSPZ Vaccine) ($N=2$). MFIs were normalized to preimmunization values. CHMI, controlled human malaria infection. ID, patient identification number. (C) PfCSP-specific IgA⁺ and IgG⁺ memory B cells (MBCs) in a sporozoite-immunized donor (donor 602). Gated on live CD19⁺CD14⁻CD3⁻CD8⁻CD56⁻CD21⁺CD27⁺IgA⁺/IgG⁺ cells, with CD27⁺CD38⁺ plasmablasts excluded. (D) Sporozoite-specific plasma IgA responses in malaria-naïve U.S. volunteers after CHMI with five *P. falciparum*-infected mosquitoes ($N=2$). MFIs were normalized to preimmunization values. (E) NANP-specific IgA plasmablasts from mice injected intradermally with transgenic *P. berghei* sporozoites expressing PfCSP (Pb-PfCSP) ($n=3$ mice per group; $N=2$ independent experiments). Cells isolated from indicated lymph nodes (LN) were analyzed 6 days after sporozoite injection. Gated on live CD138⁺IgA⁺/IgG⁺ cells. Control mice were injected with salivary gland extract from an equivalent number of mosquitoes used to obtain the sporozoites.

Of the 758 individuals followed by active surveillance for infection, only four met this criterion (Fig. 2A). Second, we identified donors with serologic evidence of sporozoite exposure and more specifically examined *P. falciparum* sporozoite-specific plasma IgA of the four PCR-negative individuals relative to the rest of the cohort. On the basis of these criteria, we chose two donors: MAD2, who tested negative by PCR 81 consecutive times over 7 years, and MAD3, who tested negative by PCR for 4 years and had the second-highest antisporozoite IgA in the cohort (Fig. 2A). Approximately 35,000 IgA⁺ B cells from MAD2 and 56,000 IgA⁺ B cells from MAD3 were screened for antibodies that bound freshly dissected *P. falciparum* NF54 sporozoites and recombinant PfCSP. We sequenced the antibody heavy and

light chains from positive B cells and identified eight recombinant IgA mAbs with confirmed binding to PfCSP and sporozoites from the two donors (Fig. 2B and table S1). Somatic (nucleotide) mutations in the VH genes of these antibodies ranged from 1.7 to 10.7%, consistent with antibody affinity maturation during germinal center reactions. Seven of eight antibodies were of the IgA1 isotype, which was expected, given the dominance of this isotype in circulation. We expressed the antibodies in their original IgA1 or IgA2 isotype without the J-chain to allow production of monomers, which is the main IgA form in blood.

We mapped the binding sites of these antibodies using peptides covering different regions of PfCSP (table S2), as previously described

Fig. 2. Naturally acquired IgA mAbs reduce sporozoite infection in vivo. (A) Time to PCR-positive *P. falciparum* blood-stage infection since study enrollment. Each individual in the cohort ($n = 758$ individuals) is represented by a horizontal line that ends when they test positive under biweekly or monthly active surveillance by finger-prick sampling, irrespective of symptoms. Individuals who were never PCR positive are shown in red (three red lines stopped early when those individuals left the study). Each red vertical mark indicates when a PCR test was performed. Inset shows sporozoite-specific plasma IgG versus IgA for the cohort, with the four PCR-negative individuals highlighted. MFI, median fluorescence intensity. (B) Schema of PfCSP and binding of IgA mAbs isolated from donors MAD2 and MAD3 to peptides from different regions of PfCSP. The heatmap shows area under the curve (AUC) from a titration of each antibody with each peptide ($N = 2$). (C) Binding of IgA or IgG mAbs from MAD2 (originally isolated as IgA) to *P. falciparum* sporozoites is shown ($N = 2$). Antibody binding was detected using the same secondary anti-light-chain antibody to allow comparison between the isotypes. (D) Sporozoite binding of IgA versus IgG mAbs, previously isolated as IgG ($N = 2$). (E) In vivo screen of IgA mAbs ($n = 5$ mice per group, except for MAD3-65, where $n = 4$). Mice were injected intravenously with 300 μg of antibody and challenged intravenously with 2000 Pb-PfCSP. Parasite liver burden was measured by IVIS 2 days later. Horizontal bars show geometric mean. The native deglycosylated form of MAD2-6 IgA was used in this assay. Differences in parasite liver burden between each antibody and the untreated control were determined using a Kruskal-Wallis test with Dunn's multiple comparison correction for panels with multiple antibodies and a two-tailed Mann-Whitney test for the panel with MAD2-302 and MAD3-23. CIS43, a highly potent antibody that targets the junction and NANP repeats (17), was used as a positive control. (F) Comparison of MAD2-6 IgA and IgG in an in vivo assay ($n = 5$ mice per group). The IgG was tested in the same experiment as screen 3 and shown here separately for clarity, with the other treatment groups shown again. Horizontal bars show geometric mean. The native deglycosylated form of MAD2-6 IgA was used in this assay. Differences in parasite liver burden between each antibody and the untreated control were determined using a Kruskal-Wallis test with Dunn's multiple comparison correction.



(16, 17). Six antibodies bound to the immunodominant NANP repeat region (Fig. 2B), and three of these were encoded by the VH3/30/VH3-33 lineage commonly seen in PfCSP-specific IgG antibodies (14, 16, 18). Antibody MAD2-6 bound to a peptide P17 that covers region I (KLKQP), which is a conserved functional site in the N terminus of PfCSP associated with cleavage before hepatocyte invasion (19). We confirmed binding of this antibody to live sporozoites by

flow cytometry (fig. S4, A and B). To determine whether the IgA isotype is important for binding, we replaced the IgA1/IgA2 backbone with IgG1 and compared their binding to *P. falciparum* sporozoites, recombinant PfCSP, and the relevant peptides using anti-light-chain secondary antibodies. Although this assay was conducted on monomeric forms of both isotypes, most of the mAbs bound better to *P. falciparum* sporozoites and PfCSP as IgA compared to IgG

(Fig. 2C and fig. S4, C and D). In contrast, when we converted previously characterized anti-PfCSP IgG mAbs (17, 20) to IgA, binding was largely unchanged (Fig. 2D). Together, these results suggest that IgA⁺ B cells undergo class switching and affinity maturation in germinal center reactions and that the IgA Fc region influences antigen binding of native IgA antibodies.

MAD2-6 IgA targets the N terminus of PfCSP and is functional in vivo

Next, we tested whether the IgA mAbs could protect in vivo by injecting them into C57BL/6 mice, challenging the mice intravenously with Pb-PfCSP sporozoites, and measuring parasite liver burden 2 days later. Initial screens with four to five mice per group revealed that two IgA antibodies, MAD2-6 and MAD3-65, resulted in the greatest reduction in parasite burden (Fig. 2E). MAD3-65 binds to the NANP repeat region, which is a known target of potent anti-PfCSP antibodies. However, the protective effect of MAD2-6, which targets the PfCSP N terminus (Fig. 2B), was unexpected, given its relatively poor binding to sporozoites (Fig. 2C). Thus, we focused subsequent in vivo experiments on MAD2-6. In vivo experiments with IgA proved technically challenging owing to rapid clearance of human IgA in mice (fig. S5A) (21, 22). We found that deglycosylation of the tailpiece *N*-glycan by treatment with PNGaseF increased antibody stability in vivo to a degree comparable to a human IgG mAb for the first 10 hours (fig. S5A). Consequently, only MAD2-6 IgA deglycosylated with PNGaseF or, through spontaneous deglycosylation after storage at 4°C, showed protective efficacy in mice (fig. S5, B to D). Although the kinetics of MAD2-6 IgG were comparable to deglycosylated MAD2-6 IgA, IgG treatment showed no protective efficacy in vivo (Fig. 2F).

Given the potential importance of this N-terminal site as a neutralizing epitope, and the fact that it is completely conserved in >2000 *P. falciparum* isolates (analyzed with Panoptes Pf3k), we extended the in vivo analysis to compare MAD2-6 with other N-terminal antibodies in a definitive experiment with 9 to 10 mice per group. It has proven difficult to isolate mAbs against the N terminus, with only a small number of mouse antibodies isolated to date. To our knowledge, mouse antibody 5D5 is the only other mAb targeting the N terminus that has been tested in vivo, with variable efficacy reported in different studies (20, 23). Furthermore, we previously isolated a rhesus IgG mAb, BL18, that binds to region I. We compared these antibodies for in vivo efficacy using the Pb-PfCSP sporozoite challenge model and found that, although MAD2-6 IgA was not as potent as the positive control antibody CIS43 (17), it was the only N-terminal-specific antibody that significantly ($P = 0.0002$) reduced parasite burden (Fig. 3A).

MAD2-6 IgA binds to a conserved site within the PfCSP N terminus

To investigate the mechanism underlying their differential potency, we mapped the binding sites of MAD2-6, 5D5, and BL18 using overlapping peptides that cover the sequence proximal to region I. MAD2-6 binds to a lysine-rich region between the binding sites of 5D5 and BL18 (Fig. 3B). Alanine scan mutagenesis revealed that these basic amino acids, specifically the KHKKLLK motif overlapping with region I, are important for MAD2-6 binding (Fig. 3C and fig. S6A). Nevertheless, some binding was retained with double and even quadruple lysine mutations, suggesting that the remaining basic amino acids contribute to binding and compensate for loss of the core motif (Fig. 3D). This lysine-rich site has been linked to PfCSP binding to

heparan sulfates on hepatocytes during sporozoite attachment (24, 25). We confirmed by enzyme-linked immunosorbent assay (ELISA) that heparin mirrors the binding pattern of MAD2-6 and binds most strongly to P17 (Fig. 3E) and that MAD2-6 and heparin compete for binding to this peptide (Fig. 3F and fig. S6B). Affinity measurements by isothermal titration calorimetry and biolayer interferometry showed that MAD2-6 IgA and IgG bind to PfCSP and P17 with comparable micromolar affinity (Fig. 3G and fig. S6, C and D). Thus, the protective activity of MAD2-6 IgA in vivo is perhaps unexpected given its relatively low affinity for PfCSP and weak binding to sporozoites in vitro. One potential explanation is that MAD2-6 binds more strongly to a transitional conformation of PfCSP displayed during hepatocyte invasion. To test this hypothesis, we measured binding of MAD2-6 to *P. falciparum* mosquito midgut sporozoites, which display PfCSP in an open conformation that is thought to be similar to its conformation during hepatocyte invasion (26). Both MAD2-6 IgA and MAD2-6 IgG bound better to midgut than salivary gland *P. falciparum* sporozoites at the highest concentration tested (Fig. 3H and fig. S7A). In contrast, a control anti-NANP repeat antibody bound twofold better to salivary gland sporozoites at the highest concentration tested (fig. S7B), suggesting that the improved binding of MAD2-6 to midgut sporozoites was not due to higher expression of surface PfCSP. To test other potential ways that MAD2-6 may interact with sporozoites, we assessed its function in several in vitro assays. MAD2-6 IgA did not trigger the CSP reaction (fig. S7, C and D) or affect *P. falciparum* sporozoite gliding motility (fig. S7, E to G), unlike the control anti-NANP repeat antibody 2A10. However, MAD2-6 IgA inhibited sporozoite invasion of hepatocytes and subsequent development of liver stage schizonts (day 5 after infection) by about 90% at a concentration of 200 µg/ml (fig. S7, H and I), consistent with its activity in vivo.

We investigated whether the N-terminal epitope targeted by MAD2-6 was commonly recognized by plasma from the Mali cohort. We observed a variable IgA and IgG response to the P17 peptide, with the majority of individuals (87 and 81% for IgA and IgG, respectively) not showing stronger antibody binding than malaria-naïve U.S. individuals (Fig. 3I). In age-adjusted analysis, we found no correlation between plasma IgA binding to peptide 17 and the risk of febrile malaria; however, for every 24% increase in IgG binding to peptide 17, there was a 50% reduction in the number of febrile malaria episodes ($P = 0.01$ after Bonferroni correction), suggesting that the MAD2-6 N-terminal epitope may be a relevant target of naturally acquired immunity to malaria.

Structural basis for recognition of the N-terminal epitope by MAD2-6 IgA Fab

To ascertain how MAD2-6 recognizes the lysine-rich site at the PfCSP N terminus, crystal structures of MAD2-6 IgA and IgG Fabs were determined in complex with short peptides that contain portions of P17 (KPKHKKLLKQ for IgA Fab and EKLRKPKHKKLLKQ peptide for IgG Fab) at 2.5 and 2.1 Å resolution, respectively (Fig. 4, fig. S8, and table S3). For simplicity, the peptides in both Fabs are numbered according to the full sequence of P17. Two copies of the Fab in both structures simultaneously recognize two different pairs of lysines, which are found in two overlapping KxxK motifs; each Fab binds on either side of the peptide (Fig. 4, A and B, and fig. S8, A and B), consistent with the redundancy observed in the peptide mutagenesis competition ELISA. The epitope targeted by MAD2-6 contains part of the epitope targeted by 5D5 and up to four residues

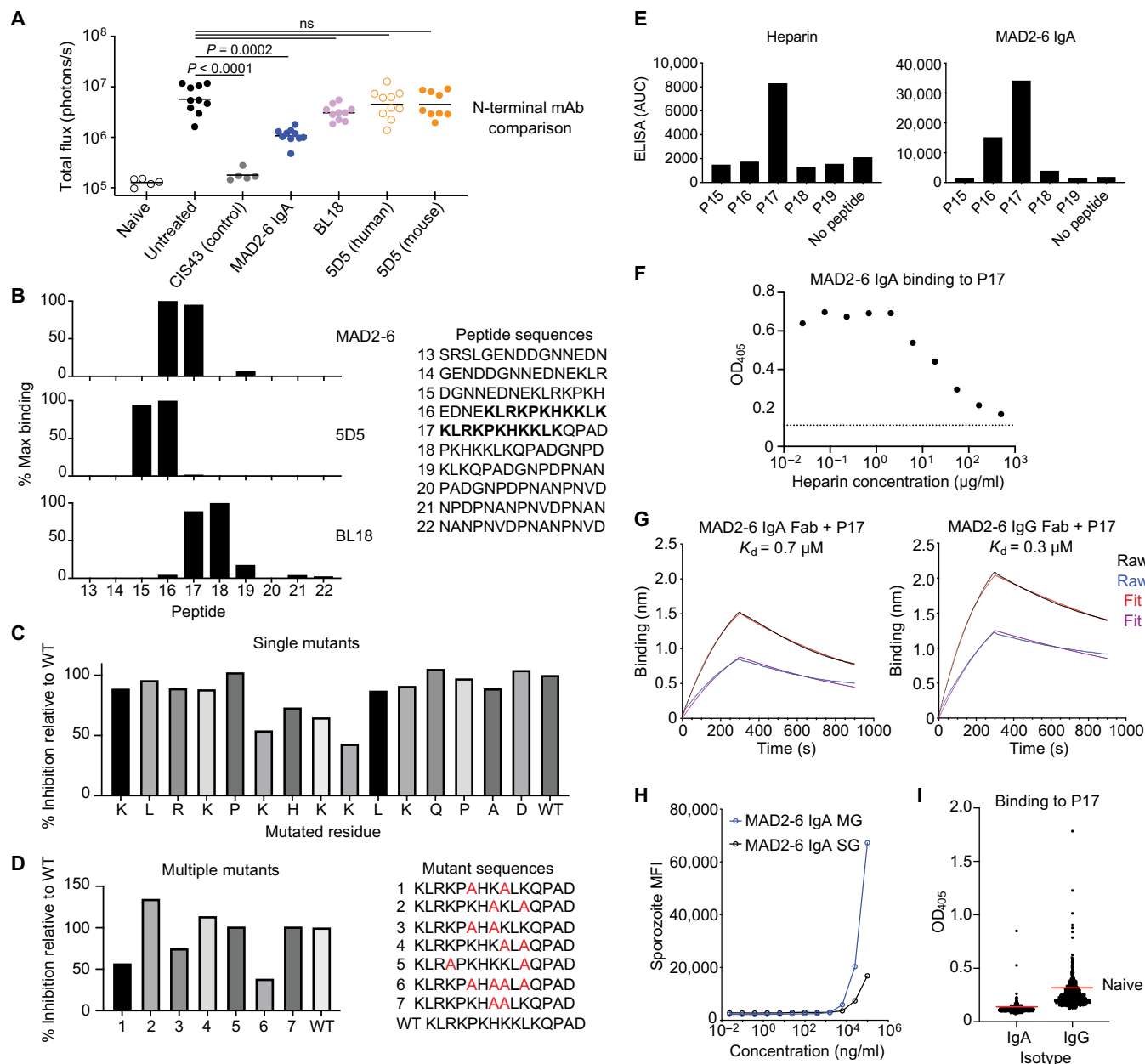


Fig. 3. MAD2-6 binds to a unique conserved region in the N terminus of CSP. (A) Comparison of efficacy between mAb 5D5 (mouse and human), mAb BL18, and deglycosylated MAD2-6 IgA in an in vivo liver burden reduction assay ($n = 10$ mice per group). Differences in liver burden between each antibody and the untreated (no antibody) control was determined using a Kruskal-Wallis test with Dunn's multiple comparison correction. Horizontal bars show geometric mean. mAb CIS43 is a positive control antibody. (B) Binding of MAD2-6 IgA, 5D5, and BL18 to peptides from the PfCSP N terminus ($N = 2$). Binding was measured by fluorescence intensity in a multiplex plate-based assay and normalized to the strongest signal for each antibody. The overlapping sequence in the two peptides bound by MAD2-6, peptides 16 and 17, is shown in bold. (C) Competition ELISA with P17 mutants carrying a single alanine substitution at each position ($N = 2$). Each bar shows the relative ability of a mutant peptide to compete with the wild-type (WT) peptide in binding to MAD2-6 IgA. (D) Competition ELISA with P17 mutants carrying multiple alanine substitutions at different lysine residues ($N = 2$). Each bar shows the relative ability of a mutant peptide to compete with the WT peptide in binding to MAD2-6 IgA. (E) Binding of heparin and MAD2-6 IgA to PfCSP N-terminal peptides, as measured by ELISA ($N = 2$). AUC, area under the curve. (F) Binding of MAD2-6 IgA to P17 with competition from heparin, as measured by ELISA ($N = 2$). The dotted line shows the baseline signal with no peptide added. OD_{405} , optical density at 405 nm. (G) Biolayer interferometry (Octet) showing MAD2-6 IgA Fab or MAD2-6 IgG binding to P17 ($N = 2$). K_d , dissociation constant. The Raw curves connect all data points, and the Fit curves are based on a model of 1:1 binding calculated using the Octet Data Analysis software. (H) Binding of MAD2-6 IgA to midgut (MG) and salivary gland (SG) *P. falciparum* sporozoites ($N = 2$). MFI, median fluorescence intensity. (I) Binding of plasma IgG, IgM, and IgA among 758 Malian individuals to peptide P17 ($N = 1$). The red lines show the mean binding based on OD_{405} of eight malaria-naïve U.S. adults.

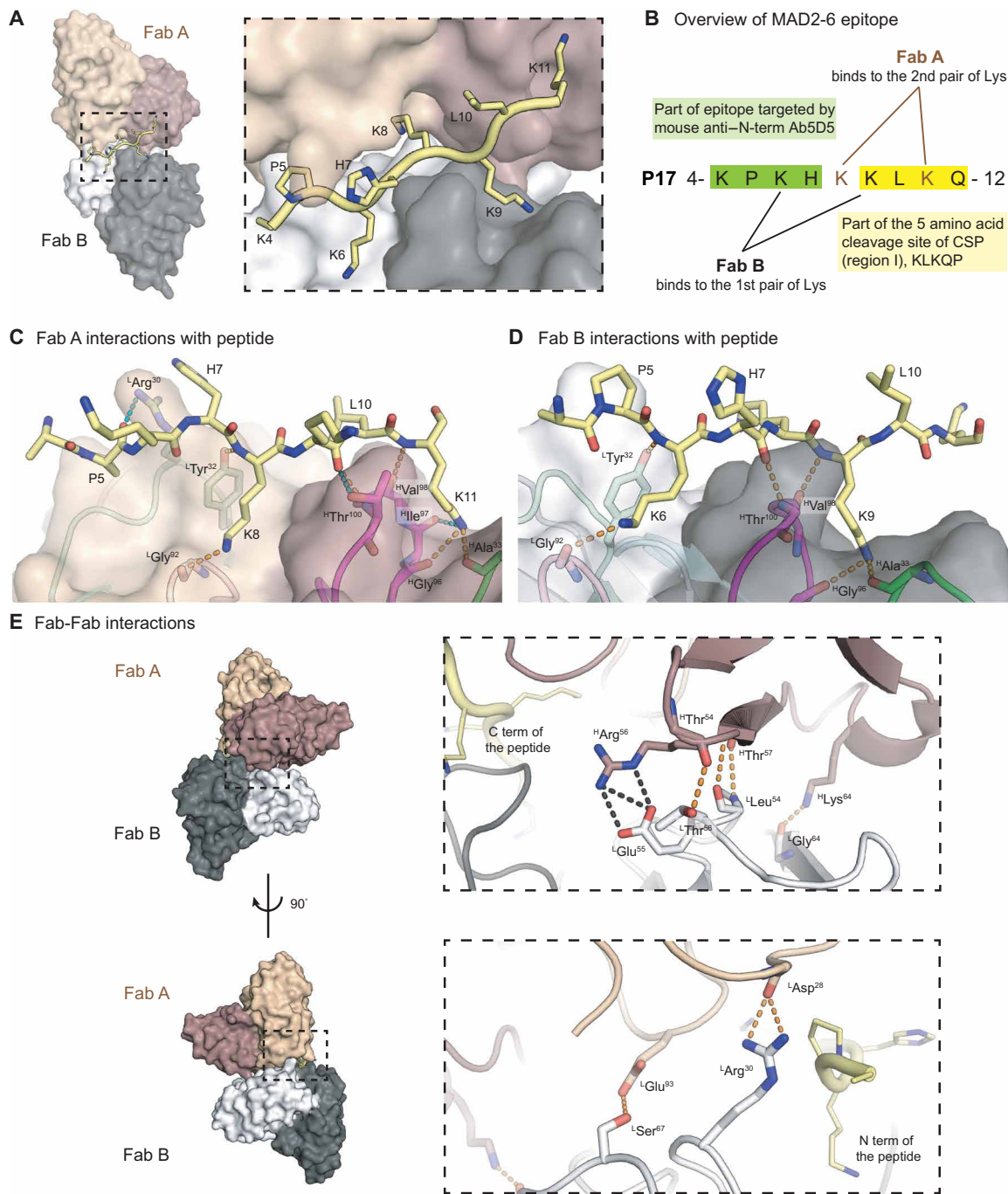


Fig. 4. Structural basis for recognition of the N-terminal epitope containing region I by MAD2-6 IgA Fab. (A) The variable domains of Fab A (heavy chain, brown; light chain, light brown) and Fab B (heavy chain, black; light chain, gray) are shown as surfaces. P17 peptide is displayed in ribbon representation with side chains as sticks. The dashed box indicates the enlarged area. Peptide residue numbers are shown. (B) Overview of MAD2-6 epitope and Fab A and Fab B binding. (C and D) Interactions of MAD2-6 IgA Fabs A (C) and B (D) with part of the P17 peptide. Fabs are displayed in ribbon representation overlaid with transparent surfaces. CDRs are colored light green, light cyan, pink, magenta, and green for CDR L1, L2, L3, H3, and H1, respectively. Hydrogen bonds (dashed lines) that are shared in both Fabs A and B are shown in orange, whereas those unique to each Fab are shown in teal. The peptide is represented as yellow sticks. Fab residue numbers are shown with superscript H and L for heavy and light chain, respectively. (E) Homotypic interactions of two MAD2-6 IgA Fabs. The Fab variable domains are shown as surfaces and ribbon representation in the enlarged box with the same coloring scheme for heavy and light chains as in (A). Black and orange dashes represent salt bridges and hydrogen bonds, respectively.

from the region I KLKQP sequence (Fig. 4B) (25). The Fab paratope is composed of complementarity-determining region (CDR) heavy (H)1, H3, light (L)1, and L3, which form two binding pockets that

accommodate Lys⁸ and Lys¹¹ in one Fab and Lys⁶ and Lys⁹ in the other Fab (Fig. 4, C and D). The interactions between each IgA Fab and their epitopes are almost identical: Hydrogen bonds are made

between the side chain of the first Lys in the KxxK motif and the CDR L3 backbone, and between the side chain of the second Lys and the CDR H1 and H3 backbone (Fig. 4, C and D). Similar pairs of peptide backbone hydrogen bonds are made to the backbone of ^HGly⁹⁶, ^HVal⁹⁸, and ^HThr¹⁰⁰ in CDR H3, as well as to the side chain of ^HThr¹⁰⁰ in Fab A (Fig. 4, C and D). Unique hydrogen bonds are also formed between ^LArg³⁰ of Fab A and the Pro5 main chain (Fig. 4C). Additional electron density for the bound peptide (slightly longer, see Materials and Methods) was observed in the MAD2-6 IgG Fab structure, which includes Gln12 from region I, allowing detection of additional hydrogen bonds between Fab B and the peptide termini. The difference in the number of hydrogen bonds to the overlapping epitope (from K4 to K11) between IgG and IgA Fabs is likely due to the higher resolution of the IgG Fab structure. Nonetheless, the region that interacts with both MAD2-6 IgA and IgG Fabs, from Lys⁴ to Lys¹¹, adopts a virtually identical conformation and Fab interactions (fig. S8, C to E). In addition, because the two copies of either MAD2-6 IgA or IgG Fabs come into close contact while simultaneously binding the peptide, they display homotypic Fab-Fab interactions, which were first observed in anti-NANP antibodies (27–29). These interactions are mainly between the heavy chain of one Fab and the light chain of the other Fab and include extensive hydrogen bonds and salt bridges between CDRs H2 and L2 (Fig. 4E and figs. S8C and S9). Most key interacting light-chain residues are present in the germline gene, whereas some of the key heavy-chain residues are somatically mutated (fig. S9). Thus, MAD2-6 exhibits an inherent propensity for homotypic Fab-Fab interactions that are further strengthened by heavy-chain somatic hypermutation, potentially explaining its low affinity *in vitro* and increased avidity *in vivo*. However, this avidity effect can be even more prominent for anti-NANP antibodies that simultaneously bind multiple epitopes formed by tandem NANP repeats (27, 29).

Although both MAD2-6 IgA and IgG Fabs exhibit identical epitope conformations, peptide interactions, and homotypic contacts, some differences are observed in their constant domains. The elbow region sequence of IgA Fab, which connects V_H to the C_{H1} domain, differs from that of the IgG Fab and allows for formation of a hydrophobic core consisting of ^HLeu¹¹, ^HPro¹¹⁶, and ^HTyr²⁰³ (fig. S8F), as previously described (30). This hydrophobic core offers potentially increased rigidity to the elbow region and is absent from Fabs of other antibody isotypes (30). Furthermore, the IgA Fab possesses two unique disulfide bonds in the constant domains. The extra, intradomain disulfide between ^HCys²¹⁴ and ^HCys¹⁹⁰ in C_{H1} may further stabilize this domain in the IgA, whereas another between the C terminus of the C_L (^LCys²¹⁴) to the middle of C_{H1} (^HCys¹²⁷) could help stabilize the constant region (fig. S8G). A corresponding interchain disulfide between ^LCys²¹⁴ and ^HCys²¹⁵ in IgG is sometimes observed in Fab crystal structures, such as anti-NANP Ab 366 (fig. S8G) (29). Thus, differences in the elbow region and constant domains may translate to greater rigidity in IgA Fabs and potentially contribute to stronger binding of MAD2-6 IgA to sporozoites, along with other factors, including higher flexibility in the IgA1 hinge region and Fc differences (31).

DISCUSSION

This study opens additional questions on the role of circulating IgA antibodies in host defense against nonmucosal pathogens. Although the IgA contribution to mucosal immunity is well documented, the origin and function of serum IgA remain unclear. Because the energy

expenditure required to maintain serum IgA rivals that of IgG (13), it is likely that circulating IgA confers a selective advantage. It is possible that serum IgA protects against bacteria that breach mucosal barriers (32). Consistent with this hypothesis, a proportion of human serum IgA targets bacteria that typically colonize mucosal surfaces (33–35). Serum IgA can be generated by long-lived IgA⁺ plasma cells of mucosal origin that migrate to bone marrow (36–38), or possibly as a result of leakage of bacterial antigens from the gut into systemic circulation, activating B cells (39). Here, we show a more direct function of circulating IgA where it contributes to protection against a nonmucosal bloodborne pathogen, which is historically attributed to IgG and IgM. These findings are consistent with a recent systems serology study reporting that IgA responses targeting the PfCSP NANP repeat region and C terminus were associated with protection in trials of the malaria vaccine candidate RTS,S/AS01 (40). Our findings suggest that B cells can class switch to IgA at the site of antigen exposure in nonmucosal tissue and undergo affinity maturation through germinal center reactions, resulting in long-lived plasma cells that produce circulating IgA antibodies against *P. falciparum* sporozoites. It will be interesting to determine the full range of function of serum IgA by investigating analogous responses to other nonmucosal pathogens.

The discovery of MAD2-6 revealed an epitope on the PfCSP N terminus that can be targeted by antibodies. All potent anti-PfCSP mAbs found to date bind to the dominant NANP repeat region, with a few antibodies binding to junctional epitopes that include variations of the core NPNA motif (14, 16–18, 41). In contrast, very few antibodies targeting the N-terminal region have been isolated (20, 26), with a recent study (23) and our own data suggesting that the best-characterized N-terminal mouse antibody, 5D5, is not protective *in vivo*. However, binding of serum antibodies to a PfCSP N-terminal peptide correlated with protection in children living in a malaria-endemic area, suggesting that regions of the N terminus can be targeted by protective antibodies (42). Our data showing a correlation between polyclonal P17-specific IgG in plasma and protection from clinical malaria support this conclusion. The MAD2-6 epitope has been implicated in binding to heparan sulfates on the hepatocyte surface (24, 25, 43) and in cleavage of the N terminus to aid sporozoite invasion (19, 44, 45). The KxxK motif bound by MAD2-6 is notably similar to heparin/heparan sulfate consensus binding motifs (25) and we confirmed that MAD2-6 and heparin compete for binding to the P17 peptide.

This study has limitations. First, although rare individuals in the Mali cohort appear to be more resistant to *P. falciparum* infection, it is unknown whether the CSP-specific IgA mAbs isolated from these individuals contribute to their apparent protection. Second, we observed an association between protection from febrile malaria and polyclonal IgG binding to the P17 peptide, although this was not observed for polyclonal IgA. Although this finding highlights the potential importance of P17 as a target of protective antibodies in general, further studies are needed to determine whether vaccine-induced or naturally acquired polyclonal IgA responses to sporozoite antigens contribute to protection. Third, we found that several malaria-naïve individuals show high IgG binding to sporozoites, and overall, these individuals have amounts of IgA and IgM binding to sporozoites that were comparable to those of malaria-exposed Malians. We speculate that some malaria-naïve individuals have memory B cells and plasma cells primed by non-*P. falciparum* antigens whose antibodies cross-react with sporozoite antigens. This hypothesis is consistent with a study reporting high mutation frequencies in PfCSP-specific B cell receptors in malaria-naïve individuals after

their first exposure to sporozoites (14), as well as several reports that PfCSP-specific antibodies are often derived from the common VH gene family VH3-30/3-33 (14, 16, 18), an observation we also made in the present study. It will be of interest in future studies to compare the biology of sporozoite-specific memory B cells of various isotypes in malaria-naïve and -experienced individuals in the context of infection and vaccination. Fourth, the precise inhibitory mechanisms of MAD2-6 IgA remain to be determined. It is possible that MAD2-6 IgA and other sporozoite-specific IgA antibodies exert some protective effect through Fc-mediated mechanisms. Because mice do not have the homolog of the human IgA Fc receptor (Fc α RI/CD89), it is unlikely that the Fc region of MAD2-6 IgA offers any advantage in the mouse model used in this study. Future studies with mice transgenic for human Fc α RI/CD89 could shed light on this question. In addition, although we provide evidence that MAD2-6 IgA competes with heparin for binding to the P17 peptide, it will also be of interest to determine whether MAD2-6 IgA inhibits proteolytic processing of the N-terminal region of PfCSP (19). Last, our findings in the mouse model suggest that sporozoites induce IgA responses in skin-draining LNs, consistent with reports of sporozoite entry into these LNs (15); however, further research is required to definitively determine the site at which IgA responses are induced by sporozoites.

In conclusion, we found that exposure to *P. falciparum* sporozoites through infection or immunization triggers a functional IgA response. Analysis of PfCSP-specific IgA mAbs from malaria-exposed individuals revealed that the antibodies targeted distinct regions of this protein. The antibody MAD2-6 IgA, which bound to a conserved site on the N terminus of PfCSP, inhibited sporozoite invasion of hepatocytes in vitro and reduced liver parasite burden in vivo. Collectively, these data reveal a role for IgA in the immune response to malaria and support further exploration of the PfCSP N terminus as a target of protective antibodies.

MATERIALS AND METHODS

Study design

The cohort study was conducted in the rural village of Kalifabougou, Mali, where *P. falciparum* transmission occurs primarily from June to December each year. The cohort has been described in detail elsewhere. Briefly, since 2011, 1187 subjects aged 1 month to 43 years have been enrolled in this ongoing study (46), and 50.8% of subjects are female. The names of potential subjects are selected at random (computer-generated randomization) from an age- and gender-stratified census (previously collected) of the entire village population of approximately 5000 inhabitants. The study team contacts selected individuals in person by visiting their respective homes and inviting them to participate in the study. Exclusion criteria at the time of screening include anemia (hemoglobin <7 g/dl); current use of antimalarials, corticosteroids, or other immunosuppressants; underlying heart disease, bleeding disorder, or other conditions that, in the judgment of the clinical investigators, could increase the risk to the study subjects; fever $\geq 37.5^{\circ}\text{C}$ or evidence of an acute infection; or currently pregnant or planning to become pregnant during the study period. There is no exclusion based on race, ethnicity, sex, or gender. Clinical malaria episodes were detected prospectively by self-referral and weekly active surveillance visits. All individuals with signs and symptoms of malaria and any *Plasmodium* parasitemia detected by light microscopy were treated according to the National

Malaria Control Program guidelines in Mali. In addition, every 2 to 4 weeks during scheduled visits, blood was collected by finger prick from all subjects to retrospectively detect asymptomatic *P. falciparum* infections by microscopic examination of blood smears and PCR analysis of dried blood spots (DBSs) on filter paper (Protein Saver 903, Whatman). Venous blood samples were collected before and after each malaria season, at the time of diagnosis of the first clinical malaria episode of each malaria season, and 7 to 10 days later. Venous blood was drawn into sodium citrate-containing cell preparation tubes (BD Biosciences) and peripheral blood mononuclear cells (PBMCs) and plasma were isolated within 2 hours according to the manufacturer's instructions. Plasma and PBMCs were stored at -80°C and in vapor-phase liquid nitrogen, respectively. For this study, we focused on 758 subjects who had plasma and PBMCs available for analysis. mAbs were isolated from two individuals in the cohort based on clinical and serological data as described in the section entitled "Isolation and characterization of IgA mAbs targeting PfCSP", and all IgA mAbs that bound to both *P. falciparum* sporozoites and PfCSP from these two individuals were characterized in this study. For mAb analysis, no randomization or blinding was performed.

Ethics approval

The Kalifabougou cohort study was approved by the Ethics Committee of the Faculty of Medicine, Pharmacy and Dentistry at the University of Sciences, Technique and Technology of Bamako, and the Institutional Review Board of the National Institute of Allergy and Infectious Diseases, National Institutes of Health (NIH IRB protocol number: 11IN126; <https://clinicaltrials.gov/>; trial number NCT01322581). Written informed consent was obtained from participants or parents or guardians of participating children before inclusion in the study.

Isolation of IgA mAbs

Cryopreserved PBMCs from the Malian cohort were thawed and stained for 20 min at 4°C in phosphate-buffered saline (PBS) + 1% fetal bovine serum with the following panel: 1:400 LIVE/DEAD Fixable Aqua, 1:50 CD14-Brilliant Violet (BV)510 (BioLegend 301842), 1:50 CD3-BV510 (BioLegend 317332), 1:50 CD56-BV510 (BioLegend 318340), 1:25 CD19-Electron Coupled Dye (ECD) (Beckman Coulter IM2708U), IgA-Alexa Fluor 647 (3 $\mu\text{g}/\text{ml}$) (Jackson ImmunoResearch 109-606-011), 1:125 IgD-phycoerythrin-Cyanine 7 (PECy7) (BD Biosciences 561314), and 1:20 IgM-peridinin-chlorophyll-protein (PerCP)-Cy5.5 (BD Biosciences 561285). Sorted IgA $^{+}$ B cells were activated as previously described (47). Briefly, cells were plated two cells per well into 384-well plates containing 10,000 irradiated 3T3-CD40L [provided by N. Doria-Rose, Mascola Laboratory, Vaccine Research Center (VRC), NIH] cells per well in a medium containing interleukin-2 (IL-2; 100 U/ml) (Roche 11147528001) and IL-21 (50 ng/ml) (Thermo Fisher Scientific, PHC0211). Cells were cultured for 2 weeks, after which supernatants were harvested and screened by high-throughput flow cytometry. The supernatants were mixed with streptavidin beads (Spherotech SVFA-2552-6K, SVFB-2552-6K, SVFA-2558-6K, and SVFB-2558-6K) coated with biotinylated full-length recombinant PfCSP protein or PfCSP peptides (see table S2 for sequence information) and incubated for 30 min at 4°C , or with *P. falciparum* NF54 sporozoites labeled with 1:2000 SYBR Green and incubated for 1 hour at 4°C . Without washing, the beads were incubated for 30 min at 4°C with either goat anti-human IgA-Dylight 405 (1 $\mu\text{g}/\text{ml}$) (Jackson ImmunoResearch 109-475-011) or goat anti-human IgA-Alexa Fluor 647 (1 $\mu\text{g}/\text{ml}$) (Jackson ImmunoResearch

were stained with 12 dilutions of each antibody, washed, and incubated with goat anti-human IgA-Alexa Fluor 647 (2.5 µg/ml) (Jackson ImmunoResearch 109-606-011) as described above. The beads were read with the iQue Screener Plus (Intellicyt) high-throughput flow cytometer and data were analyzed with FlowJo software (Tree Star). Data from titrations were analyzed by calculating area under the curve (AUC) for the titration and dividing by preimmunization AUC (VRC 314 data) or AUC for the negative control antigen (mAb data) to obtain MFI ratios. Malian plasma data were normalized by dividing MFI by the negative control antigen MFI for each plasma.

Memory B cell staining from VRC 314 trial

Cryopreserved PBMCs from the VRC 314 trial were thawed and stained for 30 min at room temperature in the dark with the following panel: 1:500 Blue LIVE/DEAD (Thermo Fisher Scientific L23105), IgA-Dylight 405 (18 µg/ml) (Jackson ImmunoResearch 109-475-011), 1:50 CD14-BV510 (BioLegend 301842), 1:50 CD3-BV510 (BioLegend 317332), 1:100 CD8-BV510 (301048), 1:50 CD56-BV510 (BioLegend 318340), 1:50 CD27-BV605 (BioLegend 302830), 1:40 CD21-BV711 (BD Biosciences 563163), 1:50 CD19-BV750 (BioLegend 302236), 1:125 IgD-PECy7 (BD Biosciences 561314), 1:20 IgM-Brilliant Ultraviolet (BUV)395 (BD Biosciences 563903), 1:125 CD38-Alexa Fluor 700 (BD Biosciences 560676), 1:40 IgG-allophycocyanin (APC) H7 (BD Biosciences 561297), 1:25 PfCSP-Brilliant Blue (BB)660, and 1:25 PfCSP-BUV737. The PfCSP probes were made by conjugating biotinylated PfCSP to streptavidin tagged with the relevant fluorescent dye. The cells were sorted using a BD FACS Aria II and analyzed with FlowJo software (Tree Star). Cells were gated on live CD19⁺ CD14⁻ CD3⁻ CD8⁻ CD56⁻ CD21⁺ CD27⁺ IgA⁺/IgG⁺, with CD27⁺⁺ CD38⁺⁺ cells excluded.

In vivo liver burden reduction assay in mice

As previously described (41), female 6- to 8-week-old B6(Cg)-Tyrc-2/J albino mice (the Jackson Laboratory) were intravenously injected with 300 µg of test mAbs diluted in a total volume of 200 µl of PBS and challenged intravenously with 2000 chimeric *P. berghei* sporozoites expressing PfCSP (Pb-PfCSP) within 2 hours. Two days after challenge, the mice were administered intraperitoneally with 150 µl of Rediject D-luciferin (30 mg/ml) (PerkinElmer) and imaged by the IVIS Spectrum in vivo imaging system (PerkinElmer) to quantify the liver-stage parasite burden. Total flux (photons/s) was measured after choosing an equivalent region of interest around each mouse liver. Liver-stage parasite burden was compared to negative control mice that did not receive a mAb and naïve mice that did not receive sporozoites. All mouse research was conducted according to NIH guidelines and approved by the VRC animal care and use ethics committee (Animal Study Protocol VRC-17-702).

Plasma binding from immunized and mosquito-bitten malaria-naïve individuals to sporozoites

P. falciparum NF54 sporozoites dissected from salivary glands were stained with 1:2000 SYBR Green and four dilutions of VRC 314 U.S. plasma (1:20, 1:100, 1:500, and 1:2500) for 30 min at 4°C, washed, and then incubated with goat anti-human IgA-Alexa Fluor 647 (Jackson ImmunoResearch 109-606-011) or goat anti-human IgG-Alexa Fluor 647 (Jackson ImmunoResearch 109-606-170) (both 2.5 µg/ml) for 30 min at 4°C. The binding data with the sporozoites were acquired with the iQue Screener Plus high-throughput flow cytometer and analyzed with FlowJo software (Tree Star).

Mouse intradermal challenge of Pb-PfCSP sporozoites

Four- to six-week-old female BALB/c mice were purchased from the Jackson Laboratory and challenged by a single intradermal injection on the left ear with 3×10^4 to 3.6×10^4 chimeric Pb-PfCSP sporozoites. Control mice were injected with a pool of matched salivary gland extract from uninfected mosquitoes. Six days later, cells were isolated from left (ipsilateral) and right (contralateral) auricular LNs, portal and celiac LNs, Peyer's patches, mesenteric LNs, and spleen for flow cytometry. Live cells were preincubated for 10 min at 4°C with 1:100 anti-CD16/CD32 mAb to block Fcγ receptors II/III and 1:1000 LIVE/DEAD Fixable aqua (Thermo Fisher Scientific L34966); stained for 15 min at 4°C with 1:250 anti-mouse CD19-APCeF780 (Invitrogen 47-0193-82), 1:250 GL7-Alexa Fluor 647 (BD Biosciences 561529), 1:250 CD95-BV421 (BD Biosciences 562633), 1:100 CD138-BV786 (BD Biosciences 740880), 1:100 IgA-PE (Invitrogen 12-4204-82), 1:100 IgG1-BUV805 (BD Biosciences 741942), 1:100 IgG2a-BUV805 (BD Biosciences 749396), 1:100 IgG2b-BUV805 (BD Biosciences 749136), 1:100 IgG3-BUV805 (BD Biosciences 749007), 1:100 NANP tetramer-fluorescein isothiocyanate (FITC), and 1:100 NANP tetramer-BV605 in BD brilliant stain buffer (BD Biosciences 563794); and fixed with BD Cytofix/Cytoperm (BD Biosciences 51-2090KZ) per the manufacturer's instructions. The NANP probes were made by conjugating biotinylated NANP to streptavidin tagged with the relevant fluorescent dye. After fixation, intracellular IgA and IgG were further stained with IgA-PE, IgG1-BUV805, IgG2a-BUV805, IgG2b-BUV805, IgG3-BUV805, NANP tetramer-FITC, and NANP tetramer-BV605 in BD brilliant stain buffer as above. Data were acquired using a BD LSRFortessa X-20 flow cytometer with FACSDiva software (BD Biosciences) and analyzed using FlowJo software (Tree Star). All mouse research was conducted according to NIH guidelines and approved by the VRC animal care and use ethics committee (Animal Study Protocol VRC-17-702).

Titration of IgA and IgG mAbs on *P. falciparum* sporozoites

P. falciparum NF54 sporozoites dissected from salivary glands or midguts were stained with 1:2000 SYBR Green and dilutions of IgA or IgG mAbs for 30 min at 4°C, washed, and then incubated with goat anti-human kappa-Alexa Fluor 647 (2.5 µg/ml) (Southern Biotech 2062-31) or goat anti-human lambda-Alexa Fluor 647 (2.5 µg/ml) (Southern Biotech 2072-31) for 30 min at 4°C. To compare the binding of MAD2-6 IgA to live and dead sporozoites, the sporozoites were stained with a range of dilutions of the antibody for 30 min at 4°C, followed by staining with IgA-Alexa Fluor 647 (2.5 µg/ml) (Jackson ImmunoResearch 109-606-011) for 30 min at 4°C. Sporozoites were labeled with mAb10-Dylight 405 (1 µg/ml) and stained with propidium iodide (5 µg/ml) loading onto the flow cytometer. Data were acquired with the iQue Screener Plus high-throughput flow cytometer and analyzed with FlowJo software (Tree Star).

Heparin and MAD2-6 binding and competition ELISA

Ninety-six-well half-area plates were coated with heparin (100 µg/ml) or MAD2-6 IgA, incubated at 37°C for 1 hour, and blocked with 1% bovine serum albumin (BSA) in PBS. Serially diluted P14-P19 PfCSP peptides and recombinant PfCSP (see table S2 for sequence information) were added to the plate and incubated for 1 hour at room temperature. Next, 1:500 goat anti-human IgG Fc-alkaline phosphatase (Southern Biotech 2048-04) was added to the plate for a 1-hour incubation, followed by p-nitrophenyl phosphate (p-NPP) substrate

(Sigma-Aldrich). The plates were read with the EnSpire plate reader (PerkinElmer) at 405 nm after 1 hour.

In competition experiments, plates were coated with MAD2-6 IgA (100 µg/ml) or IgG overnight at 4°C and blocked with 1% BSA in PBS. A mixture of heparin (Fresenius Kabi 401586J) at a range of concentrations and biotinylated P17 (0.5 µg/ml) was added to the plates. Next, streptavidin-alkaline phosphatase (Southern Biotech 7100-04) was added to the plate, and the plates were developed and read after 30 min as described above.

Multiplex plate-based fluorescence assay (U-Plex)

Mapping of MAD2-6, 5D5, and BL18 mAbs was performed using PfCSP overlapping peptides (peptides 13 to 22) that were 15 amino acids in length (GenScript) and overlapped by 11 residues spanning the N-terminal region of PfCSP. The assay was performed using the MSD U-Plex Assay platform (Meso Scale Discovery) according to the manufacturer's instructions.

Biolayer interferometry

Kinetics of antibody binding to PfCSP peptides were measured using streptavidin-capture biosensors in the Octet Red384 system (fortéBio). Assays were performed with agitation at 30°C. mAbs were plated in solid black tilt-well 384-well plates (Geiger Bio-One). Loading of the biotinylated P17 peptide was done for 300 s, followed by immersing the biosensors into buffer (PBS + 1% BSA) for 60 s to assess baseline assay drift. Association with whole IgG (serially diluted from 2 µM to 31 nM) was performed for 300 s, followed by dissociation in buffer for 600 s. Data analysis and curve fitting were performed using Octet Data Analysis software. Experimental data were fitted with the binding equations describing a 1:1 heterologous ligand interaction. Global analyses of the complete datasets, assuming binding was reversible (full dissociation), were carried out using nonlinear least-squares fitting allowing a single set of binding parameters to be obtained simultaneously for all concentrations of a given mAb dilution series.

Structural biology

MAD2-6 IgG Fab was concentrated to 10 mg/ml and mixed with the EKLRKPKHKHKLKQ peptide, which overlaps with P17 (KLRKPKH-KKLKQPAD) recognized by MAD2-6 mAb in the initial screening, in a 5:1 molar ratio of peptide to Fab. Upon identifying the minimal epitope of MAD2-6 IgG Fab, MAD2-6 IgA Fab was crystallized with a shorter peptide, KPKHKHKLKQ, at the same concentration and molar ratio. The peptides used for cocrystallization were ordered from Innopep Inc. with a purity of >98% and contained chlorine counterions. Crystal screening was carried out using a high-throughput, robotic CrystalMation system (Rigaku) at The Scripps Research Institute, which was based on the sitting drop vapor diffusion method with 35 µl of reservoir solution and each drop consisting of 0.1 µl of protein +0.1 µl of precipitant. High-quality crystals of the MAD2-6 IgG Fab-peptide co-complex diffracted to 2.14 Å and were grown in a reservoir solution containing 2.4 M ammonium sulfate and 0.1 M MES (pH 6.0). Crystals of the MAD2-6 IgA Fab-peptide co-complex diffracted to 2.50 Å and were grown in a well solution containing 20% polyethylene glycol 3350 and 0.2 M potassium citrate (pH 8.3). Crystals for both co-complexes were grown at 20°C and appeared after 3 days. MAD2-6 IgG and IgA Fab co-complex crystals were cryoprotected by soaking in a well solution supplemented with 20% glycerol and 20% ethylene glycol, respectively, before being flash-cooled

in liquid nitrogen. X-ray diffraction data were collected at the Advanced Proton Source beamline 23ID-B. The datasets were indexed, integrated, and scaled using the HKL-2000 package (54). The structures were determined by molecular replacement (MR) using Phaser (55), with a crystal structure of Fab311 [(18), PDB 6AXK] as a search model for MAD2-6 IgG Fab. The MAD2-6 IgA Fab structure was solved using the variable domain from the MAD2-6 IgG Fab and the constant domain from PDB 3M8O (30) as the MR search models. Structure refinement was performed using phenix.refine (56), and iterations of refinement were performed using Coot (57). Amino acid residues of the Fabs were numbered using the Kabat system, and the structures were validated using MolProbity (58). Hydrogen bonds were assessed with the program HBPLUS (59). The crystal structures have been deposited in the PDB database with PDB ID 7K75 and 7K76 for MAD2-6 IgA and IgG Fabs, respectively.

Statistical analysis

Associations between plasma IgA binding to sporozoites, plasma IgG binding to sporozoites, plasma IgA binding to PfCSP, and donor age were evaluated using a two-tailed Pearson's correlation. Segmented regression of plasma IgA versus age was performed using the "segmented" package library in R, and the median age was used as the initial value of the breakpoint for the two segments. The association between P17-specific IgA and IgG ($n = 525$ subjects) and the number of febrile malaria episodes during the ensuing transmission season was determined using age-adjusted Poisson regression analysis, with Bonferroni correction. In the in vivo experiment comparing the efficacy of N-terminal antibodies, differences in parasite liver burden between each antibody and the no mAb control were determined using the Kruskal-Wallis with Dunn's multiple comparison test for panels with multiple antibodies and the two-tailed Mann-Whitney test for the panel with MAD2-302 and MAD3-23. Total fluorescence intensity of CSP-stained sporozoites and trails between the MAD2-6, 2A10, and buffer control were compared using one-way analysis of variance (ANOVA) with Dunnett's multiple comparisons. In the figure legends, N refers to the number of independent experiments unless stated otherwise.

SUPPLEMENTARY MATERIALS

stm.sciencemag.org/cgi/content/full/13/599/eabg2344/DC1

Materials and Methods

Figs. S1 to S9

Tables S1 to S3

Data file S1

References (60–65)

[View/request a protocol for this paper from Bio-protocol.](#)

REFERENCES AND NOTES

1. World Health Organization, *World Malaria Report 2020* (World Health Organization, 2020).
2. P. D. Crompton, J. Moebius, S. Portugal, M. Waisberg, G. Hart, L. S. Garver, L. H. Miller, C. Barillas-Mury, S. K. Pierce, Malaria immunity in man and mosquito: Insights into unsolved mysteries of a deadly infectious disease. *Annu. Rev. Immunol.* **32**, 157–187 (2014).
3. T. M. Tran, S. Li, S. Doumbo, D. Doumbo, C.-Y. Huang, S. Dia, A. Bathily, J. Sangala, Y. Kone, A. Traore, M. Niangaly, C. Dara, K. Kayentao, A. Ongoiba, O. K. Doumbo, B. Traore, P. D. Crompton, An intensive longitudinal cohort study of Malian children and adults reveals no evidence of acquired immunity to *Plasmodium falciparum* infection. *Clin. Infect. Dis.* **57**, 40–47 (2013).
4. RTS,S Clinical Trials Partnership, First results of phase 3 trial of RTS,S/AS01 malaria vaccine in African children. *N. Engl. J. Med.* **365**, 1863–1875 (2011).
5. RTS,S Clinical Trials Partnership, A phase 3 trial of RTS,S/AS01 malaria vaccine in African infants. *N. Engl. J. Med.* **367**, 2284–2295 (2012).

6. RTS,S Clinical Trials Partnership, Efficacy and safety of RTS,S/AS01 malaria vaccine with or without a booster dose in infants and children in Africa: Final results of a phase 3, individually randomised, controlled trial. *Lancet* **386**, 31–45 (2015).
7. I. A. Cockburn, R. A. Seder, Malaria prevention: From immunological concepts to effective vaccines and protective antibodies. *Nat. Immunol.* **19**, 1199–1211 (2018).
8. J. Tan, L. Piccoli, A. Lanzavecchia, The antibody response to *Plasmodium falciparum*: Cues for vaccine design and the discovery of receptor-based antibodies. *Annu. Rev. Immunol.* **37**, 225–246 (2019).
9. S. Cohen, I. A. McGregor, S. Carrington, Gamma-globulin and acquired immunity to human malaria. *Nature* **192**, 733–737 (1961).
10. C. D. Thouvenel, M. F. Fontana, J. Netland, A. T. Krishnamurthy, K. K. Takehara, Y. Chen, S. Singh, K. Miura, G. J. Keitany, E. M. Lynch, S. Portugal, M. C. Miranda, N. P. King, J. M. Kollman, P. D. Crompton, C. A. Long, M. Pancera, D. J. Rawlings, M. Pepper, Multimeric antibodies from antigen-specific human IgM⁺ memory B cells restrict *Plasmodium* parasites. *J. Exp. Med.* **218**, e20200942 (2021).
11. C. S. Hopp, P. Sekar, A. Diouf, K. Miura, K. Boswell, C. M. Tipton, M. E. Peterson, M. J. Chambers, S. Andrews, J. Lu, J. Tan, S. Li, S. Doumbo, K. Kayentao, A. Ongoiba, B. Traore, S. Portugal, P. D. Sun, C. Long, R. A. Koup, E. O. Long, A. B. McDermott, P. D. Crompton, *Plasmodium falciparum*-specific IgM B cells dominate in children, expand with malaria, and produce functional IgM. *J. Exp. Med.* **218**, e20200901 (2021).
12. A. J. Macpherson, K. D. McCoy, F.-E. Johansen, P. Brandtzaeg, The immune geography of IgA induction and function. *Mucosal Immunol.* **1**, 11–22 (2008).
13. J. M. Woof, M. A. Kerr, The function of immunoglobulin A in immunity. *J. Pathol.* **208**, 270–282 (2006).
14. R. Murugan, L. Buchauer, G. Triller, K. Kreschel, G. Costa, G. P. Marti, K. Imkeller, C. E. Busse, S. Chakravarty, B. K. L. Sim, S. L. Hoffman, E. A. Levashina, P. G. Kremsner, B. Mordmüller, T. Höfer, H. Wardemann, Clonal selection drives protective memory B cell responses in controlled human malaria infection. *Sci. Immunol.* **3**, eaap8029 (2018).
15. R. Amino, S. Thiherge, B. Martin, S. Celli, S. Shorte, F. Frischknecht, R. Ménard, Quantitative imaging of *Plasmodium* transmission from mosquito to mammal. *Nat. Med.* **12**, 220–224 (2006).
16. J. Tan, B. K. Sack, D. Oyen, I. Zenklusen, L. Piccoli, S. Barbieri, M. Foglierini, C. S. Fregni, J. Marcandalli, S. Jongso, S. Abdulla, L. Perez, G. Corradin, L. Varani, F. Sallusto, B. K. L. Sim, S. L. Hoffman, S. H. I. Kappe, C. Daubenberger, I. A. Wilson, A. Lanzavecchia, A public antibody lineage that potentially inhibits malaria infection through dual binding to the circumsporozoite protein. *Nat. Med.* **24**, 401–407 (2018).
17. N. K. Kisalu, A. H. Idris, C. Weidle, Y. Flores-García, B. J. Flynn, B. K. Sack, S. Murphy, A. Schön, E. Freire, J. R. Francica, A. B. Miller, J. Gregory, S. March, H.-X. Liao, B. F. Haynes, K. Wiehe, A. M. Trama, K. O. Saunders, M. A. Gladde, A. Monroe, M. Bonsignori, M. Kanekiyo, A. K. Wheatley, A. B. McDermott, S. K. Farney, G.-Y. Chuang, B. Zhang, N. Kc, S. Chakravarty, P. D. Kwong, P. S. Sillis, S. H. I. Kappe, B. K. L. Sim, S. L. Hoffman, F. Zavala, M. Pancera, R. A. Seder, A human monoclonal antibody prevents malaria infection by targeting a new site of vulnerability on the parasite. *Nat. Med.* **24**, 408–416 (2018).
18. D. Oyen, J. L. Torres, U. Wille-Reece, C. F. Ockenhouse, D. Emerling, J. Glanville, W. Volkmuth, Y. Flores-García, F. Zavala, A. B. Ward, C. R. King, I. A. Wilson, Structural basis for antibody recognition of the NANP repeats in *Plasmodium falciparum* circumsporozoite protein. *Proc. Natl. Acad. Sci. U.S.A.* **114**, E10438–E10445 (2017).
19. A. Coppi, C. Pinzon-Ortiz, C. Hutter, P. Sillis, The *Plasmodium* circumsporozoite protein is proteolytically processed during cell invasion. *J. Exp. Med.* **201**, 27–33 (2005).
20. D. A. Espinosa, G. M. Gutierrez, M. Rojas-López, A. R. Noe, L. Shi, S.-W. Tse, P. Sillis, F. Zavala, Proteolytic cleavage of the *Plasmodium falciparum* circumsporozoite protein is a target of protective antibodies. *J. Infect. Dis.* **212**, 1111–1119 (2015).
21. A. Rifai, K. Fadden, S. L. Morrison, K. R. Chintalacharuvu, The N-glycans determine the differential blood clearance and hepatic uptake of human immunoglobulin (Ig)A1 and IgA2 isotypes. *J. Exp. Med.* **191**, 2171–2182 (2000).
22. T. N. Lombana, S. Rajan, J. A. Zorn, D. Mandikian, E. C. Chen, A. Estevez, V. Yip, D. D. Bravo, W. Phung, F. Farahi, S. Vijayar, S. Lee, A. Gill, W. Sandoval, J. Wang, C. Ciferri, C. A. Boswell, M. L. Matsumoto, C. Spiess, Production, characterization, and in vivo half-life extension of polymeric IgA molecules in mice. *MAbs* **11**, 1122–1138 (2019).
23. E. Thai, G. Costa, A. Weyrich, R. Murugan, D. Oyen, Y. Flores-García, K. Prieto, A. Bosch, A. Valleriani, N. C. Wu, T. Pholcharee, S. W. Scally, I. A. Wilson, H. Wardemann, J.-P. Julien, E. A. Levashina, A high-affinity antibody against the CSP N-terminal domain lacks *Plasmodium falciparum* inhibitory activity. *J. Exp. Med.* **217**, e20200061 (2020).
24. C. Pinzon-Ortiz, J. Friedman, J. Esko, P. Sillis, The binding of the circumsporozoite protein to cell surface heparan sulfate proteoglycans is required for *Plasmodium* sporozoite attachment to target cells. *J. Biol. Chem.* **276**, 26784–26791 (2001).
25. J. B. Ancsin, R. Kisilevsky, A binding site for highly sulfated heparan sulfate is identified in the N terminus of the circumsporozoite protein. Significance for malarial sporozoite attachment to hepatocytes. *J. Biol. Chem.* **279**, 21824–21832 (2004).
26. R. Herrera, C. Anderson, K. Kumar, A. Molina-Cruz, V. Nguyen, M. Burkhardt, K. Reiter, R. Shimp Jr., R. F. Howard, P. Srinivasan, M. J. Nold, D. Ragheb, L. Shi, M. DeCotiis, J. Aebig, L. Lambert, K. M. Rausch, O. Muratova, A. Jin, S. G. Reed, P. Sinnis, C. Barillas-Mury, P. E. Duffy, N. J. MacDonald, D. L. Narum, Reversible conformational change in the *Plasmodium falciparum* circumsporozoite protein masks its adhesion domains. *Infect. Immun.* **83**, 3771–3780 (2015).
27. K. Imkeller, S. W. Scally, A. Bosch, G. P. Marti, G. Costa, G. Triller, R. Murugan, V. Renna, H. Jumaa, P. G. Kremsner, B. K. L. Sim, S. L. Hoffman, B. Mordmüller, E. Levashina, J.-P. Julien, H. Wardemann, Antihomotypic affinity maturation improves human B cell responses against a repetitive epitope. *Science* **360**, 1358–1362 (2018).
28. D. Oyen, J. L. Torres, C. A. Cottrell, C. R. King, I. A. Wilson, A. B. Ward, Cryo-EM structure of *P. falciparum* circumsporozoite protein with a vaccine-elicited antibody is stabilized by somatically mutated inter-Fab contacts. *Sci. Adv.* **4**, eaau8529 (2018).
29. T. Pholcharee, D. Oyen, Y. Flores-García, G. Gonzalez-Paez, Z. Han, K. L. Williams, W. Volkmuth, D. Emerling, E. Locke, C. R. King, F. Zavala, I. A. Wilson, Structural and biophysical correlation of anti-NANP antibodies with in vivo protection against *P. falciparum*. *Nat. Comm.* **12**, 1063 (2021).
30. A. Correa, F. Trajtenberg, G. Obal, O. Pritsch, G. Dighiero, P. Oppezio, A. Buschiazio, Structure of a human IgA1 Fab fragment at 1.55Å resolution: Potential effect of the constant domains on antigen-affinity modulation. *Acta Crystallogr. D* **69**, 388–397 (2013).
31. G. K. Hui, D. W. Wright, O. L. Vennard, L. E. Rayner, M. Pang, S. C. Yeo, J. Gor, K. Molyneux, J. Barratt, S. J. Perkins, The solution structures of native and patient monomeric human IgA1 reveal asymmetric extended structures: Implications for function and IgAN disease. *Biochem. J.* **471**, 167–185 (2015).
32. S. K. Davis, K. J. Selva, S. J. Kent, A. W. Chung, Serum IgA Fc effector functions in infectious disease and cancer. *Immunol. Cell Biol.* **98**, 276–286 (2020).
33. I. R. Cohen, L. C. Norris, Natural human antibodies to Gram-negative bacteria: Immunoglobulins G, A, and M. *Science* **152**, 1257–1259 (1966).
34. H. Scott, T. O. Rognum, T. Midtvedt, P. Brandtzaeg, Age-related changes of human serum antibodies to dietary and colonic bacterial antigens measured by an enzyme-linked immunosorbent assay. *Acta Pathol. Microbiol. Immunol. Scand. C* **93**, 65–70 (1985).
35. A. Haas, K. Zimmermann, F. Graw, E. Slack, P. Rusert, B. Ledergerber, W. Bossart, R. Weber, M. C. Thurnheer, M. Battegay, B. Hirschele, P. Vernazza, N. Patuto, A. J. Macpherson, H. F. Günthard, A. Oxenius; Swiss HIV Cohort Study, Systemic antibody responses to gut commensal bacteria during chronic HIV-1 infection. *Gut* **60**, 1506–1519 (2011).
36. H. E. Mei, T. Yoshida, W. Sime, F. Hiepe, K. Thiele, R. A. Manz, A. Radbruch, T. Dörner, Blood-borne human plasma cells in steady state are derived from mucosal immune responses. *Blood* **113**, 2461–2469 (2009).
37. M. Bemark, H. Hazanov, A. Strömberg, R. Komban, J. Holmqvist, S. Köster, J. Mattsson, P. Sikora, R. Mehr, N. Y. Lycke, Limited clonal relatedness between gut IgA plasma cells and memory B cells after oral immunization. *Nat. Commun.* **7**, 12698 (2016).
38. A. Lemke, M. Kraft, K. Roth, R. Riedel, D. Lammerding, A. E. Hauser, Long-lived plasma cells are generated in mucosal immune responses and contribute to the bone marrow plasma cell pool in mice. *Mucosal Immunol.* **9**, 83–97 (2016).
39. K. Zimmermann, A. Haas, A. Oxenius, Systemic antibody responses to gut microbes in health and disease. *Gut Microbes* **3**, 42–47 (2012).
40. T. J. Suscovich, J. K. Fallon, J. Das, A. R. Demas, J. Crain, C. H. Linde, A. Michell, H. Natarajan, C. Arevalo, T. Broge, T. Linnekin, V. Kulkarni, R. Lu, M. D. Slein, C. Luedemann, M. Marquette, S. March, J. Weiner, S. Gregory, M. Coccia, Y. Flores-García, F. Zavala, M. E. Ackerman, E. Bergmann-Leitner, J. Hendriks, J. Sadoff, S. Dutta, S. N. Bhatia, D. A. Lauffenburger, E. Jongert, U. Wille-Reece, G. Alter, Mapping functional humoral correlates of protection against malaria challenge following RTS,S/AS01 vaccination. *Sci. Transl. Med.* **12**, eabb4757 (2020).
41. L. T. Wang, L. S. Pereira, Y. Flores-García, J. O'Connor, B. J. Flynn, A. Schön, N. K. Hurlburt, M. Dillon, A. S. P. Yang, A. Fabra-García, A. H. Idris, B. T. Mayer, M. W. Gerber, R. Gottardo, R. D. Mason, N. Cavett, R. B. Ballard, N. K. Kisalu, A. Molina-Cruz, J. Nelson, R. Vistein, C. Barillas-Mury, R. Amino, D. Baker, N. P. King, R. W. Sauerwein, M. Pancera, I. A. Cockburn, F. Zavala, J. R. Francica, R. A. Seder, A potent anti-malarial human monoclonal antibody targets circumsporozoite protein minor repeats and neutralizes sporozoites in the liver. *Immunity* **53**, 733–744.e8 (2020).
42. S. E. Bongfen, P. M. Ntsama, S. Offner, T. Smith, I. Felger, M. Tanner, P. Alonso, I. Nebie, J. F. Romero, O. Silvie, R. Torgler, G. Corradin, The N-terminal domain of *Plasmodium falciparum* circumsporozoite protein represents a target of protective immunity. *Vaccine* **27**, 328–335 (2009).
43. J. Zhao, P. Bhanot, J. Hu, Q. Wang, A comprehensive analysis of *Plasmodium* circumsporozoite protein binding to hepatocytes. *PLoS ONE* **11**, e0161607 (2016).
44. A. Coppi, R. Tewari, J. R. Bishop, B. L. Bennett, R. Lawrence, J. D. Esko, O. Billker, P. Sinnis, Heparan sulfate proteoglycans provide a signal to *Plasmodium* sporozoites to stop migrating and productively invade host cells. *Cell Host Microbe* **2**, 316–327 (2007).

45. A. Coppi, R. Natarajan, G. Pradel, B. L. Bennett, E. R. James, M. A. Roggero, G. Corradin, C. Persson, R. Tewari, P. Sinnis, The malaria circumsporozoite protein has two functional domains, each with distinct roles as sporozoites journey from mosquito to mammalian host. *J. Exp. Med.* **208**, 341–356 (2011).
46. T. M. Tran, R. Guha, S. Portugal, J. Skinner, A. Ongoiba, J. Bhardwaj, M. Jones, J. Moebius, P. Venepally, S. Doumbo, E. A. DeRiso, S. Li, K. Vijayan, S. L. Anzick, G. T. Hart, E. M. O'Connell, O. K. Doumbo, A. Kaushansky, G. Alter, P. L. Felgner, H. Lorenzi, K. Kayentao, B. Traore, E. F. Kirkness, P. D. Crompton, A molecular signature in blood reveals a role for p53 in regulating malaria-induced inflammation. *Immunity* **51**, 750–765. e10 (2019).
47. J. Huang, N. A. Doria-Rose, N. S. Longo, L. Laub, C.-L. Lin, E. Turk, B. H. Kang, S. A. Migueles, R. T. Bailer, J. R. Mascola, M. Connors, Isolation of human monoclonal antibodies from peripheral blood B cells. *Nat. Protoc.* **8**, 1907–1915 (2013).
48. T. Tiller, E. Meffre, S. Yurasov, M. Tsuiji, M. C. Nussenzweig, H. Wardemann, Efficient generation of monoclonal antibodies from single human B cells by single cell RT-PCR and expression vector cloning. *J. Immunol. Methods* **329**, 112–124 (2008).
49. M.-P. Lefranc, Immunoglobulin and T cell receptor genes: IMGT® and the birth and rise of immunoinformatics. *Front. Immunol.* **5**, 22 (2014).
50. G. Snounou, S. Viriyakosol, X. P. Zhu, W. Jarra, L. Pinheiro, V. E. do Rosario, S. Thaithong, K. N. Brown, High sensitivity of detection of human malaria parasites by the use of nested polymerase chain reaction. *Mol. Biochem. Parasitol.* **61**, 315–320 (1993).
51. K. E. Lyke, A. S. Ishizuka, A. A. Berry, S. Chakravarty, A. DeZure, M. E. Enama, E. R. James, P. F. Billingsley, A. Gunasekera, A. Manoj, M. Li, A. J. Ruben, T. Li, A. G. Eappen, R. E. Stafford, N. KC, T. Murshedkar, F. H. Mendoza, I. J. Gordon, K. L. Zephir, L. A. Holman, S. H. Plummer, C. S. Hendel, L. Novik, P. J. M. Costner, J. G. Saunders, N. M. Berkowitz, B. J. Flynn, M. C. Nason, L. S. Garver, M. B. Laurens, C. V. Plowe, T. L. Richie, B. S. Graham, M. Roederer, B. K. L. Sim, J. E. Ledgerwood, S. L. Hoffman, R. A. Seder, Attenuated PfSPZ Vaccine induces strain-transcending T cells and durable protection against heterologous controlled human malaria infection. *Proc. Natl. Acad. Sci. U.S.A.* **114**, 2711–2716 (2017).
52. K. Moll, A. Kaneko, A. Scherf, M. Wahlgren, *Methods in Malaria Research* (Bie Resources, ed. 6, 2013).
53. C. Crosnier, M. Wanaguru, B. McDade, F. H. Osier, K. Marsh, J. C. Rayner, G. J. Wright, A library of functional recombinant cell-surface and secreted *P. falciparum* merozoite proteins. *Mol. Cell. Proteomics* **12**, 3976–3986 (2013).
54. Z. Otwinowski, W. Minor, Processing of x-ray diffraction data collected in oscillation mode. *Methods Enzymol.* **276**, 307–326 (1997).
55. A. J. McCoy, R. W. Grosse-Kunstleve, P. D. Adams, M. D. Winn, L. C. Storoni, R. J. Read, Phaser crystallographic software. *J. Appl. Cryst.* **40**, 658–674 (2007).
56. P. D. Adams, P. V. Afonine, G. Bunkóczy, V. B. Chen, I. W. Davis, N. Echols, J. J. Headd, L.-W. Hung, G. J. Kapral, R. W. Grosse-Kunstleve, A. J. McCoy, N. W. Moriarty, R. Oeffner, R. J. Read, D. C. Richardson, J. S. Richardson, T. C. Terwilliger, P. H. Zwart, PHENIX: A comprehensive Python-based system for macromolecular structure solution. *Acta Crystallogr. D* **66**, 213–221 (2010).
57. P. Emsley, B. Lohkamp, W. G. Scott, K. Cowtan, Features and development of Coot. *Acta Crystallogr. D* **66**, 486–501 (2010).
58. V. B. Chen, W. B. Arendall III, J. J. Headd, D. A. Keedy, R. M. Immormino, G. J. Kapral, L. W. Murray, J. S. Richardson, D. C. Richardson, *MolProbity: All-atom structure validation for macromolecular crystallography*. *Acta Crystallogr. D* **66**, 12–21 (2010).
59. I. K. McDonald, J. M. Thornton, Satisfying hydrogen bonding potential in proteins. *J. Mol. Biol.* **238**, 777–793 (1994).
60. L. Jaenicke, A rapid micromethod for the determination of nitrogen and phosphate in biological material. *Anal. Biochem.* **61**, 623–627 (1974).
61. W. Trager, J. Jensen, Human malaria parasites in continuous culture. *Science* **193**, 673–675 (1976).
62. J. W. Zolg, A. J. MacLeod, I. H. Dickson, J. G. Scaife, *Plasmodium falciparum*: Modifications of the in vitro culture conditions improving parasitic yields. *J. Parasitol.* **68**, 1072–1080 (1982).
63. A. Roth, S. P. Maher, A. J. Conway, R. Ubalee, V. Chaumeau, C. Andolina, S. A. Kaba, A. Vantoux, M. A. Bakowski, R. Thomson-Luque, S. R. Adapa, N. Singh, S. J. Barnes, C. A. Cooper, M. Rouillier, C. W. McNamara, S. A. Mikolajczak, N. Sather, B. Witkowski, B. Campo, S. H. I. Kappe, D. E. Lanar, F. Nosten, S. Davidson, R. H. Y. Jiang, D. E. Kyle, J. H. Adams, A comprehensive model for assessment of liver stage therapies targeting *Plasmodium vivax* and *Plasmodium falciparum*. *Nat. Commun.* **9**, 1837 (2018).
64. T. L. Alves e Silva, A. Radtke, A. Balaban, T. V. Pascini, Z. R. Pala, A. Roth, P. H. Alvarenga, Y. J. Jeong, J. Olivas, A. K. Ghosh, H. Bui, B. S. Pybus, P. Sinnis, M. Jacobs-Lorena, J. Vega-Rodríguez, The fibrinolytic system enables the onset of *Plasmodium* infection in the mosquito vector and the mammalian host. *Sci. Adv.* **7**, eabe3362 (2021).
65. J. R. Francica, Z. Sheng, Z. Zhang, Y. Nishimura, M. Shingai, A. Ramesh, B. F. Keele, S. D. Schmidt, B. J. Flynn, S. Darko, R. M. Lynch, T. Yamamoto, R. Matus-Nicodemus, D. Wolinsky, NISC Comparative Sequencing Program, M. Nason, N. M. Valiante, P. Malyala, E. D. Gregorio, S. W. Barnett, M. Singh, D. T. O'Hagan, R. A. Koup, J. R. Mascola, M. A. Martin, T. B. Kepler, D. C. Douek, L. Shapiro, R. A. Seder, Analysis of immunoglobulin transcripts and hypermutation following SHIVAD8 infection and protein-plus-adjuvant immunization. *Nat. Commun.* **6**, 6565 (2015).

Acknowledgments: We thank the residents of Kalifabougou, Mali, for participating in this study; B. K. L. Sim and S. L. Hoffman (Sanaria Inc.) for providing the PfSPZ Vaccine; G. Wright and N. Muller-Sienherth (University of York, Wellcome Trust Sanger Institute) for providing recombinant CD4 and MSP1; and L. Krymskaya (Division of Intramural Research, NIAID) for assistance with sorting memory B cells. **Funding:** This work was supported by the Division of Intramural Research and the Vaccine Research Center, National Institute of Allergy and Infectious Diseases, National Institutes of Health. The work was partially supported by the Bill & Melinda Gates Foundation, grant OPP1170236 (to I.A.W.); the National Cancer Institute, National Institutes of Health, under contract no. HHSN261200800001E (to A.S.); Military Infectious Diseases Research Program (MIDRP) proposal Q0480_19_WR_CS_OC (to P.J.L. and A.R.); NIH through a Johns Hopkins Malaria Institute Fellowship (R01 AI132359, to P.S. and S.K.); and the Wellcome Trust, grant 204689/Z/16/Z (to J.T.). **Author contributions:** J.T., H.C., R.A.S., and P.D.C. conceived and designed the study. J.T. and H.C. isolated and characterized monoclonal antibodies. T.P. and D.O. performed structural analysis. L.S.P. and M.D. performed in vivo experiments. S.D., D.D., S.L., K.K., A.O., and B.T. managed the collection of clinical data and biospecimens. B.J.F. conducted peptide mapping. A.S. performed isothermal titration calorimetry assays. S.K. performed gliding and CSP reaction assays. S.O.A. performed the hepatocyte invasion assay. R.V. screened for PfCSP-positive B cells. L.W. performed memory B cell activation assay. J.S. performed statistics. M.P. performed ELISAs on cohort samples. S.L. performed PCRs to detect malaria infection. A.H.I. handled immunized cohorts. A.M.-C. and C.B.-M. provided sporozoites. M.Z. and L.R.O. performed mass spectrometry. P.J.L. obtained funding for the hepatocyte invasion assay. A.R., P.S., J.R.F., I.A.W., R.A.S., and P.D.C. aided in data analysis. **Competing interests:** J.T., H.C., R.A.S., and P.D.C. have submitted U.S. Patent Application No. 63/041,439, filed 19 June 2020, describing antibody MAD2-6. All other authors declare that they have no competing interests. **Data and materials availability:** All data associated with this study are present in the paper or the Supplementary Materials. The sequences of the antibody heavy and light chains have been deposited in NCBI GenBank under accession numbers MZ076644 to MZ076659. Crystal structures have been deposited in the PDB database with PDB ID 7K75 and 7K76 for MAD2-6 IgA and IgG Fabs, respectively. The IgA monoclonal antibodies are covered by a material transfer agreement (NIAID/NIH). Correspondence and requests for materials should be addressed to J.T. and P.D.C.

Submitted 18 December 2020

Accepted 21 April 2021

Published 23 June 2021

10.1126/scitranslmed.abg2344

Citation: J. Tan, H. Cho, T. Pholcharee, L. S. Pereira, S. Doumbo, D. Doumtabe, B. J. Flynn, A. Schön, S. Kanatani, S. O. Aylor, D. Oyen, R. Vistein, L. Wang, M. Dillon, J. Skinner, M. Peterson, S. Li, A. H. Idris, A. Molina-Cruz, M. Zhao, L. R. Olano, P. J. Lee, A. Roth, P. Sinnis, C. Barillas-Mury, K. Kayentao, A. Ongoiba, J. R. Francica, B. Traore, I. A. Wilson, R. A. Seder, P. D. Crompton, Functional human IgA targets a conserved site on malaria sporozoites. *Sci. Transl. Med.* **13**, eabg2344 (2021).

Functional human IgA targets a conserved site on malaria sporozoites

Joshua TanHyeseon ChoTossapol PholchareeLais S. PereiraSafiatou DoumboDidier DoumtabeBarbara J. FlynnArne SchönSachie KanataniSamantha O. AylorDavid OyenRachel VisteinLawrence WangMarlon DillonJeff SkinnerMary PetersonShanping LiAzza H. IdrisAlvaro Molina-CruzMing ZhaoLisa Renee OlanoPatricia J. LeeAlison RothPhotini SinnisCarolina Barillas-MuryKassoum KayentaoAissata OngoibaJoseph R. FrancicaBoubacar TraoreIlan A. WilsonRobert A. SederPeter D. Crompton

Sci. Transl. Med., 13 (599), eabg2344. • DOI: 10.1126/scitranslmed.abg2344

A role for IgA in malaria

Immunoglobulin (Ig)A is known to play a protective role against pathogens at mucosal surfaces. However, the protective effects of IgA in the serum are less well understood, particularly in the context of pathogens such as *Plasmodium falciparum*. To address this question, Tan *et al.* isolated and characterized serum IgA from three independent cohorts of humans exposed to *P. falciparum*. The authors further studied IgA antibodies isolated from individuals who were consistently resistant to malaria, finding that they were protective in mouse models *in vivo* and bound to a conserved site on sporozoites. Together, these results established a role for serum IgA in the context of malaria and identified a region of the circumsporozoite protein as a target for these protective antibodies.

View the article online

<https://www.science.org/doi/10.1126/scitranslmed.abg2344>

Permissions

<https://www.science.org/help/reprints-and-permissions>

Use of this article is subject to the [Terms of service](#)

Science Translational Medicine (ISSN 1946-6242) is published by the American Association for the Advancement of Science. 1200 New York Avenue NW, Washington, DC 20005. The title *Science Translational Medicine* is a registered trademark of AAAS. Copyright © 2021 The Authors, some rights reserved; exclusive licensee American Association for the Advancement of Science. No claim to original U.S. Government Works